Journal of NUCLEAR SCIENCE and TECHNOLOGY, Vol. 33, No. 8, p. 609–619 (August 1996)

Acceleration Mechanism of Vertical Displacement Event and its Amelioration in Tokamak Disruptions

Yukiharu NAKAMURA†, Ryuji YOSHINO,

*Naka Fusion Research Establishment, Japan Atomic Energy Research Institute**

Neil POMPHREY and Stephen C. JARDIN

*Princeton Plasma Physics Laboratory, Princeton University***

(Received April 18, 1996)

Vertical displacement events (VDEs), which are frequently observed in disruptive discharges of elongated tokamaks, are investigated using the Tokamak Simulation Code. We show that disruption events such as a sudden plasma pressure drop (β_p collapse) and the subsequent plasma current quench (I_p quench) can accelerate VDEs due to the adverse destabilizing effect of the resistive shell, which has previously been thought to stabilize VDEs. In a tokamak with a surrounding shell which is asymmetric with respect to the geometric midplane, the I_p quench also causes an additional VDE acceleration due to the vertical imbalance of the attractive force. While the shell-geometry characterizes the VDE dynamics, the growth rate of VDEs depends strongly on the magnitude of the β_p collapse, the speed of the I_p quench and the n-index of the plasma equilibrium just before the disruption. An amelioration of I_p quench-induced VDEs was experimentally established in the JT-60U tokamak by optimizing the vertical location of the plasma just prior to the disruption. The JT-60U vacuum vessel is shown to be suitable for preventing the β_p collapse-induced VDE.

KEYWORDS: ***vertical displacement event, tokamak disruption, plasma pressure drop, plasma current quench, positional instability, tokamak simulation code, n-index, JT-60U tokamak, stabilizing shell, eddy currents, halo current***

I. Introduction

In investigating tokamak disruptions we seek to improve our understanding to the point where disruption-free discharges are realizable, or at worst, soft landing disruptions occasionally occur. Many experimental and theoretical works have sought this goal[1]-[4], however because of the device-dependent complexity of disruption processes no reliable control technique has yet been developed. Although experimentally observed major disruptions can have different causes and involve a complex sequence of events, typical common features include a strong energy quench (β_p collapse) followed by a rapid plasma current decay (I_p quench) and a coincident fast plasma displacement away from the horizontal midplane—a vertical displacement event (VDE)[2][5][6]. A rapid I_p quench induces large eddy currents in the vacuum vessel which in turn lead to significant electromagnetic forces[7]. A VDE can also cause serious wall damage since any active feedback system will become incapable of maintaining position control during the disruption, and hence the unstable plasma with high internal energy can contact plasma-facing components in the vacuum vessel[8].

In recent years, several major experiments like JET[8], DIII-D[5], ASDEX-Upgrade[6] and JT-60U[3] have focused research on vertically elongated plasmas, because elongated plasmas have improved the confinement properties and increased plasma beta limits[9]. However, elongated plasmas have the drawback of positional instability[10]-[12], or VDEs. The experimental growth rates of VDEs during disruptions is measured to be three or more times higher than the values predicted by positional stability theory including the stabilizing effect of the vacuum vessel[1][3][8]. A close correlation between the I_p quench rate and the VDE rate was shown experimentally in the JT-60U tokamak for low β_p, ohmically heated plasmas; *i.e.* a rapid I_p quench was shown to enhance the VDE[3]. It is also well known that large Halo currents with both toroidal and poloidal components can appear during disruptions in the open flux scrape-off layer (SOL) just outside the main plasma (Halo region)[2][5][6][13][14]. Halo currents with up to 20-30 % of the initial plasma current have been observed in DIII-D and JET disruptions[5][14], and have resulted in substantial electromagnetic forces, that were larger in magnitude than forces caused by the I_p quench. It

* *Naka-machi, Naka-gun, Ibaraki-ken 311-01.*
** *Princeton, New Jersey 08543, USA.*
† Corresponding author, Tel. +81-29-270-7351,
Fax +81-29-270-7419,
E-mail: nakamura@expert1.naka.jaeri.go.jp

has also been pointed out that the Halo current can significantly affect plasma dynamics in DIII-D disruptive discharges[2], that is, Halo currents are believed to suppress VDEs[2][13]. However, despite the progress in understanding what accelerates and decelerates VDEs, all VDE mechanisms during disruptions have still not been clearly identified and a general method for avoiding or controlling VDEs has not yet been proposed. In next-generation tokamak fusion devices such as ITER[6][12], successful operation requires a detailed understanding of VDE mechanisms and a development of techniques for softening the VDE.

In this paper, we describe in detail the acceleration mechanisms of VDEs induced by a rapid I_p quench, which is a typical event in major disruptions terminating a low β_p plasma discharge, and by a strong β_p collapse, which is typical in minor disruptions of high β_p tokamaks. Moreover, we intend to develop a practical control technique to prevent VDEs, and propose guide-lines for design criteria of the VDE-free tokamak. To clarify the VDE mechanism, self-consistent nonlinear simulations of disruption dynamics are carried out numerically using the Tokamak Simulation Code (TSC)[15], which is capable of modelling the realistic VDE evolution including the passive effect of resistive shells. Chapter II describes the numerical model used in the TSC simulation and the fundamental characteristics of the JT-60U positional stability. In Chap.III, the acceleration mechanisms of the I_p quench-induced VDE and the β_p collapse-induced VDE in the JT-60U tokamak are discussed. In Chap.IV, we present an amelioration technique for the I_p quench-induced VDE which has now been successfully demonstrated in JT-60U tokamak experiments. In addition, the effects of the shell-geometry on the β_p collapse-induced VDE are discussed in detail. Finally, our conclusions are given in Chap.V.

II. Simulation Model

Here, we describe the TSC code[15], which is capable of modelling the deformable plasma behavior of a free-boundary axisymmetric tokamak including plasma transport[16] and many realistic control functions, including an active feedback system and passive stabilization due to resistive shells. The detailed modelling of the JT-60U tokamak is also described and the fundamental characteristics of the positional instability are discussed.

1. TSC Code

In the TSC code, modified magnetohydrodynamic equations are solved inside a computational domain that includes a plasma region, a vacuum region, a specified number of solid conductors and a resistive wall. Green's function techniques allow specification of the boundary conditions at infinity. The form of the modified momentum equation used is:

$$\frac{\partial \boldsymbol{m}}{\partial t} + \boldsymbol{F}_v(\boldsymbol{m}) = \boldsymbol{J} \times \boldsymbol{B} - \nabla p. \tag{1}$$

Here, $\boldsymbol{m}$ is the plasma momentum density $M_i n \boldsymbol{v}$. Instead of the convective derivative term, a specific form of the plasma viscosity operator:

$$\boldsymbol{F}_v(\boldsymbol{m}) = -\nu_1[\nabla^2 \boldsymbol{m} - \nabla(\nabla \cdot \boldsymbol{m})] - \nu_2 \nabla(\nabla \cdot \boldsymbol{m}), \tag{2}$$

is introduced in the left-hand side of Eq.(1). The mass M_i and viscosities, ν_1, ν_2, are chosen to achieve critical damping of the modified Alfven waves. This makes the time integration feasible while keeping the left side of Eq.(1) small compared with the terms on the right side. In order to obtain physically correct results, the TSC model must nearly satisfy the static equilibrium condition: $\boldsymbol{J} \times \boldsymbol{B} = \nabla p$, with an integration time step that is much longer than the Alfven time scale. It must be verified *a posteriori* that the effects of the modified inertial terms are small and that the physical results are independent of the fictitious mass and viscosity values.

The magnetic field is represented in the usual way for an axisymmetric system: $\boldsymbol{B} = \nabla\phi \times \nabla\Psi + g\nabla\phi$, where ϕ is the symmetry angle. Faraday's law and Ohm's law: $\boldsymbol{E} + \boldsymbol{v} \times \boldsymbol{B} = \boldsymbol{R}$ yield evolution equations for the poloidal flux Ψ and toroidal field function g. The inhomogeneous term $\boldsymbol{R}$ contains the effects of nonideal dissipations. The static form of Eq.(1) is exactly equivalent to the well known Grad-Shafranov equation[17]:

$$\Delta^* \Psi + \mu_0 x^2 \frac{d}{d\Psi} p(\Psi) + \frac{1}{2} \cdot \frac{d}{d\Psi} g^2(\Psi) \equiv 0. \tag{3}$$

Here, $\Delta^* \equiv x^2 \nabla \cdot (x^{-2} \nabla)$ is the standard toroidal elliptic operator and x the radius in cylindrical coordinates.

Although TSC has many capabilities for simulating realistic plasma behavior, we focus here on the axisymmetric dynamics of toroidal plasmas interacting electromagnetically with resistive shells. This is because our interest mainly lies in the rapid process during disruptions whose time scales are much faster than the L/R time of the resistive shell. During a VDE evolution, the coupling of the plasma with the poloidal field (PF) coil circuits can be neglected. Therefore, the PF coils are assumed to provide only a static magnetic field, *i.e.*, we can neglect both the active feedback and the passive response of the PF coil system.

The inclusion of the detailed plasma transport including impurity influx and degradation of energy confinement is beyond the scope of our computational work. Therefore, in order to introduce disruption dynamics, the plasma pressure is given a prescribed time-dependence. The functional forms of the plasma pressure profile and plasma density profile are assumed to remain unchanged during the TSC simulation. These are given by $p(\overline{\Psi}) = p_0 \overline{\Psi}^{3/2}$ and $n(\overline{\Psi}) = n_0 \overline{\Psi}$, respectively. Here, $\overline{\Psi}$ $(= (\Psi - \Psi_s)/(\Psi_{\text{axis}} - \Psi_s))$ is the normalized poloidal flux.

In this paper, we also neglect the effect of the Halo current on the VDE dynamics, because our main inter-

est lies in the initial phase of the disruption where Halo currents are nearly absent according to measurements in JT-60U experiment[13], DIII-D[5], and JET[14]. Another reason for neglecting the Halo currents in the present study is that we are interested in mechanisms that accelerate the VDEs, whereas Halo currents are known to mitigate VDEs.

2. JT-60U Tokamak

(1) TSC Modeling

JT-60U[1] is a vertically elongated, bottom-diverted, single-null (SN) tokamak with an egg-shaped vacuum vessel that plays the role of the resistive shell. **Figure 1** illustrates the TSC configuration of a typical plasma equilibrium and the nominal conductors that model the JT-60U PF coil systems and the vacuum vessel, which is slightly up-down asymmetric with respect to the midplane. The dominant up-down antisymmetric current mode of the vacuum vessel, which stabilizes vertical displacement, has a decay time constant of about 8 ms. The computational domain is the square box spanning 1.5 to 5.5 m in the major radius direction and −2.0 to 2.0 m in the vertical direction. This domain is divided into (80×80) grids with equal spacing of 5 cm. Major plasma parameters in Fig. 1 are the following: plasma current I_p=1.5 MA, toroidal magnetic field B_t=3.5 T, poloidal beta β_p=0.2, plasma internal inductance l_i=1.5, and the location of magnetic axis is R=3.33 m and Z=0.0 m. The shape of the plasma cross section is characterized by the elongation κ=1.5 and the triangularity δ=0.09.

(2) Positional Stability

According to the linear stability theory using a simple model of rigid shifts of circular-shaped plasmas, the linear growth rate γ of positional instabilities is given as a function of the magnetic field decay n-index and the stability index n_s[11]:

$$n + n_s \frac{\gamma\tau_s}{1+\gamma\tau_s} = 0. \tag{4}$$

Here, τ_s is the effective skin time of the resistive shell. The decay n-index is a measure of the curvature of the vertical magnetic field B_Z needed for equilibrium, defined by

$$n = -\frac{R}{B_Z}\cdot\frac{\partial B_Z}{\partial R}. \tag{5}$$

The stability index n_s, which was first defined by Fukuyama *et al.*[11], is a measure of the positional stability. It is a function of the shell-geometry and the plasma parameter $\Lambda(=\ln(8R_p/a)+\beta_p+l_i/2-3/2)$, *i.e.*,

$$n_s = \frac{2}{\Lambda}\cdot\frac{R_p^2}{b^2}\left(1-\frac{a^2}{b^2}\right)^{-1}. \tag{6}$$

Here, R_p is the plasma major radius, a the minor radius, and b the mean minor radius of the resistive shell. Although Eqs.(4) and (6) cannot express the detailed characteristics of positional instabilities of highly elongated tokamaks with a non circular-shaped resistive shell like Fig. 1, they provide a useful guide to the essential character of positional instabilities. For instance, Eqs.(4) and (6) indicate that high β_p plasmas are more unstable, and that the more the decay index decreases, the more the growth rate of the positional instability increases.

Figure 2 shows the linear growth rate for the plasma with the same parameters in Fig. 1 as a function of the n-index. The closed circles show the growth rates obtained by TSC, while the solid curve is the one estimated using Eq.(4) provided that the curve coincides with the respective closed circles of TSC growth rates. In evaluating the TSC simulation-growth rates, first an initial static equilibrium was obtained consistent with plasma parameters of interest. Next, the plasma was given a small vertical displacement ($Z\sim-1.0$ cm) as an initial condition for the dynamic simulation. The TSC time-evolution of the vertical displacement was then followed during the period of linear growth. The vertical growth without any significant changes of I_p, β_p, l_i, and plasma deformation was

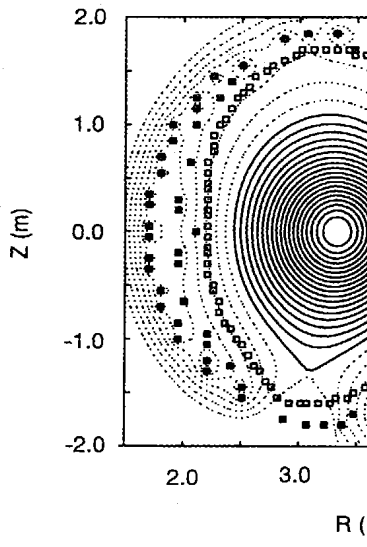

Fig. 1 TSC configuration of JT-60U plasma equilibrium with PF coil system (closed boxes) and vacuum vessel (open boxes)

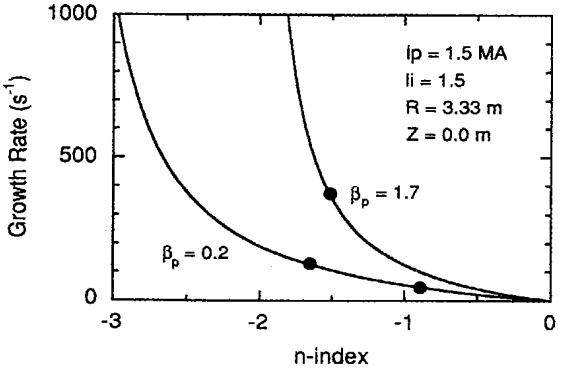

Fig. 2 Linear growth rate of JT-60U positional instability as a function of the decay n-index

est lies in the initial phase of the disruption where Halo currents are nearly absent according to measurements in JT-60U experiment[13], DIII-D[5], and JET[14]. Another reason for neglecting the Halo currents in the present study is that we are interested in mechanisms that accelerate the VDEs, whereas Halo currents are known to mitigate VDEs.

2. JT-60U Tokamak

(1) TSC Modeling

JT-60U[1] is a vertically elongated, bottom-diverted, single-null (SN) tokamak with an egg-shaped vacuum vessel that plays the role of the resistive shell. **Figure 1** illustrates the TSC configuration of a typical plasma equilibrium and the nominal conductors that model the JT-60U PF coil systems and the vacuum vessel, which is slightly up-down asymmetric with respect to the midplane. The dominant up-down antisymmetric current mode of the vacuum vessel, which stabilizes vertical displacement, has a decay time constant of about 8 ms. The computational domain is the square box spanning 1.5 to 5.5 m in the major radius direction and −2.0 to 2.0 m in the vertical direction. This domain is divided into (80×80) grids with equal spacing of 5 cm. Major plasma parameters in Fig. 1 are the following: plasma current I_p=1.5 MA, toroidal magnetic field B_t=3.5 T, poloidal beta β_p=0.2, plasma internal inductance l_i=1.5, and the location of magnetic axis is R=3.33 m and Z=0.0 m. The shape of the plasma cross section is characterized by the elongation κ=1.5 and the triangularity δ=0.09.

(2) Positional Stability

According to the linear stability theory using a simple model of rigid shifts of circular-shaped plasmas, the linear growth rate γ of positional instabilities is given as a function of the magnetic field decay n-index and the stability index n_s[11]:

$$n + n_s \frac{\gamma\tau_s}{1+\gamma\tau_s} = 0. \tag{4}$$

Here, τ_s is the effective skin time of the resistive shell. The decay n-index is a measure of the curvature of the vertical magnetic field B_Z needed for equilibrium, defined by

$$n = -\frac{R}{B_Z}\cdot\frac{\partial B_Z}{\partial R}. \tag{5}$$

The stability index n_s, which was first defined by Fukuyama *et al.*[11], is a measure of the positional stability. It is a function of the shell-geometry and the plasma parameter Λ(=ln($8R_p/a$)+β_p+$l_i/2$−3/2), *i.e.*,

$$n_s = \frac{2}{\Lambda}\cdot\frac{R_p^2}{b^2}\left(1-\frac{a^2}{b^2}\right)^{-1}. \tag{6}$$

Here, R_p is the plasma major radius, a the minor radius, and b the mean minor radius of the resistive shell. Although Eqs.(4) and (6) cannot express the detailed characteristics of positional instabilities of highly elongated tokamaks with a non circular-shaped resistive shell like Fig. 1, they provide a useful guide to the essential character of positional instabilities. For instance, Eqs.(4) and (6) indicate that high β_p plasmas are more unstable, and that the more the decay index decreases, the more the growth rate of the positional instability increases.

Figure 2 shows the linear growth rate for the plasma with the same parameters in Fig. 1 as a function of the n-index. The closed circles show the growth rates obtained by TSC, while the solid curve is the one estimated using Eq.(4) provided that the curve coincides with the respective closed circles of TSC growth rates. In evaluating the TSC simulation-growth rates, first an initial static equilibrium was obtained consistent with plasma parameters of interest. Next, the plasma was given a small vertical displacement ($Z\sim-1.0$ cm) as an initial condition for the dynamic simulation. The TSC time-evolution of the vertical displacement was then followed during the period of linear growth. The vertical growth without any significant changes of I_p, β_p, l_i, and plasma deformation was

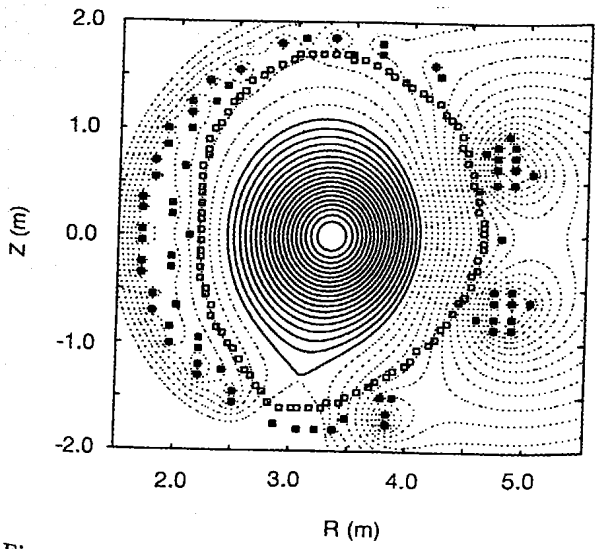

Fig. 1 TSC configuration of JT-60U plasma equilibrium with PF coil system (closed boxes) and vacuum vessel (open boxes)

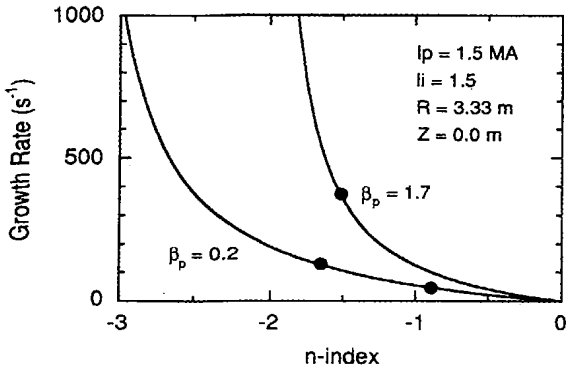

Fig. 2 Linear growth rate of JT-60U positional instability as a function of the decay n-index

carefully monitored. While the growth rate of the low β_p plasma with β_p=0.2 is relatively small (γ=128 s^{-1} at n=−1.6), the high β_p plasma with β_p=1.7 gives a larger growth rate (γ=375 s^{-1} at n=−1.5). We note that the stabilizing effect of the vacuum vessel depends strongly on the decay n-index. For example, the growth rate as predicted by the linear stability theory[11] for β_p=0.2 is γ=46 s^{-1} at n=−0.9. This nonlinear dependence of the growth rate on the n-index has important consequences when investigating the acceleration mechanism of VDEs during disruptions, as is discussed in the next chapter.

Ⅲ. Acceleration Mechanism in JT-60U

This chapter describes TSC simulations of acceleration mechanisms of the I_p quench-induced VDE[18] and of the β_p collapse-induced VDE[19].

1. VDE due to Plasma Current Quench

(1) JT-60U Disruptive Discharges

Figure 3 shows a typical time-evolution of the magnetic axis and the plasma current as experimentally observed in a JT-60U disruptive discharge (displayed by dotted lines)[20]. The corresponding TSC simulated time-evolution is shown to agree well with the experiment (bold lines) during the period of 11.347 s<t<11.359 s. A loss of plasma stored energy (energy quench) occurred at t=11.347 s and lasted for about 200 μs. Prior to the energy quench, the plasma equilibrium was elongated (n=−1.6)*, with plasma parameters I_p=1.5 MA, l_i=1.5, and β_p=0.2. In the TSC simulation, the electron temperature after the energy quench was specified to be 100 eV as indicated by the JT-60U ECE measurement[18], and this temperature reproduced the experimental I_p quench rate of 50 s^{-1}. During the energy quench, a flattening of the plasma current profile resulted in a small increase of the plasma current. In the final stage of current termination, after t=11.36 s, Halo current with up 30% of the total plasma current was induced, however, almost no net Halo current was observed during the period of t<11.357 s[18]. We attribute the discrepancy of trajectories between the TSC simulation and the experiment at the final stage to the fact that this TSC simulation neglects the Halo current effect. The discrepancy between the data and the simulation is consistent with the fact that Halo currents mitigate the fast VDE.

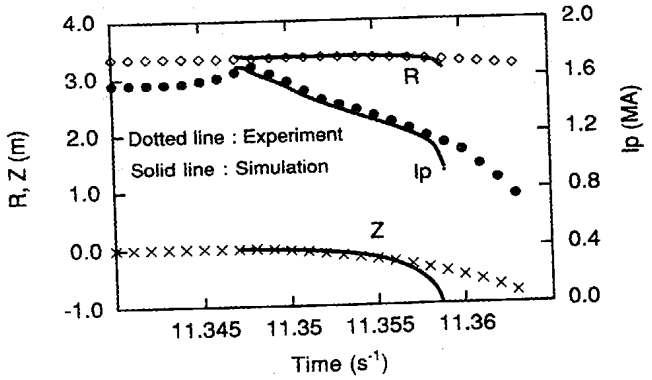

Fig. 3 Time-evolutions of magnetic axis (R, Z) and plasma current I_p in JT-60U disruption of the elongated plasma (n=−1.6) with I_p=1.5 MA and β_p=0.2

The VDE rate at the initial stage of t=11.348 - 11.356 s was about 425 s^{-1}, which is 3.4 times faster than the linear growth rate of the positional instability previously estimated as 128 s^{-1}. It is well recognized that the shrinkage of the plasma current channel is a contributing mechanism for VDE enchancements[6]. During the TSC simulation, we observed a peaking of the plasma current profile by amount of Δl_i=0.5, while the elongation remains approximately constant. However, it was also shown that the shrinkage of the plasma current channel is not the prime effect which accelerates VDEs, because the VDE enhancement due to the observed increase of Δl_i=0.5 is only 50 s^{-1}[18]. In what follows, we discuss another candidate for an acceleration mechanism of the I_p quench-induced VDE.

Data collected from many JT-60U disruptive discharges indicates a close correlation between the I_p quench rate and the VDE rate as shown in **Fig. 4**[18]. Data points with relatively low I_p quench rates correspond to density limit type disruptions, while those with relatively high I_p quench rates correspond to error field type disruptions. The predisruption values of plasma current ranged from 1 to 3 MA and both the elongated (n=−1.6) and the standard (n=−0.9) configurations are included in Fig. 4. It is clear that the VDE rate increases as the I_p quench rate increases. The explanation of these characteristic features of experimental results are the objects of the TSC studies described in the present paper.

(2) VDE Mechanism

We carried out a series of TSC simulations for a variety of plasma configurations to study the correlation

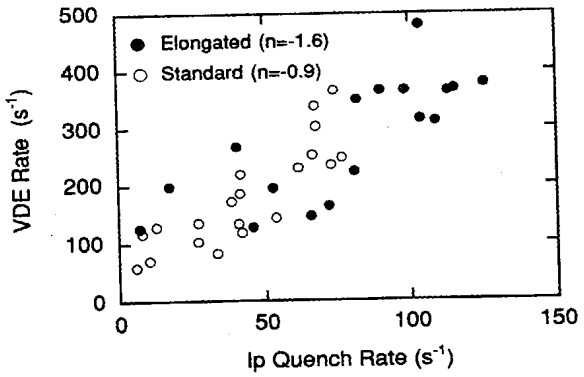

Fig. 4 Experimental VDE rate as a function of I_p quench rate

* The JT-60U PF coil system is capable of producing two different plasma configurations, *i.e.*, the standard configuration (n=−0.9) and the elongated configuration (n=−1.6)[18].

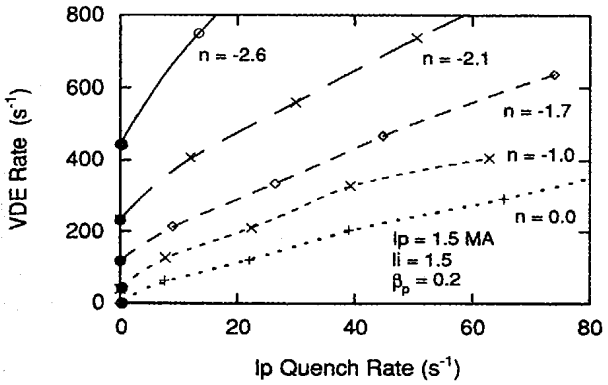

Fig. 5 VDE rate as a function of I_p quench rate by TSC simulation

between VDE rates and I_p quench rates. The results are displayed in **Fig. 5**. The main plasma parameters used in this study were I_p=1.5 MA, β_p=0.2, l_i=1.5, and elongations κ ranged from 1.1 to 1.6. Configurations with nearly circular plasmas (n=0.0) and highly elongated plasmas (n=−2.1, −2.6) were created by introducing artificial quadrupole magnetic field moments, which are constant in time. VDE rates at the zero I_p quench rate correspond to growth rates of positional instability that are consistent with Fig. 2. The remarkable features of Fig. 5 are summarized as follows: (1) VDE rates of all configurations increase as the I_p quench rate increases (consistent with the JT-60U experiments shown in Fig. 4). (2) An I_p quench causes a VDE-like vertical displacement even for the circular plasma, which should be positionally stable. (3) For highly elongated configurations (*e.g.*, n=−2.6), an I_p quench substantially accelerates the VDEs compared with configurations with a small elongation.

We monitored the decay n-index at the magnetic axis in the TSC simulation and found a n-index degradation Δn from its equilibrium value. The rapid I_p quench induces a large eddy current on the vacuum vessel. For highly elongated configurations, these eddy currents form in the top and bottom sections of the vacuum vessel. These eddy currents produce an additional quadrupole moment of the magnetic field and hence result in a degradation of the n-index. From the fundamental characteristics of the positional instability shown in Fig. 2, it is clear that the degradation of the n-index leads to a higher growth rate. In **Table 1**, the observed degradations Δn and the resultant enhancements of the positional instability $\Delta\gamma$, which are estimated with help of Fig. 2, are listed for the case of an I_p quench rate of 40 s^{-1}. Table 1 implies that while the degradation Δn for the circular plasma is nearly absent, the magnitude of Δn increases as the n-index before an energy quench decreases, then the resultant n-index $n+\Delta n$ provides a substantial enhancement of VDEs. For the case of the fictitious configuration with n=−2.6, whose growth rate

Table 1 Degradation of n-index due to I_p quench and resultant destabilization of positional instability obtained from TSC simulation

n-index/$\gamma^{\dagger 1}$ /(s^{-1})	$\gamma^{*\dagger 2}$ (s^{-1})	$\Delta n^{\dagger 3}$	$\Delta\gamma^{\dagger 4}$ (s^{-1})	$\gamma+\Delta\gamma^{\dagger 5}$ (s^{-1})
0.0/ 0	200	0.0	0	0
−1.0/ 50	300	−0.2	30	80
−1.6/130	430	−0.3	70	200
−2.1/230	640	−0.3	150	380
−2.6/430	1,100	−0.4	450	880

†1 Growth rate of pure positional instability read from Fig. 2
†2 VDE rate for the case of I_p quench rate of 40 s^{-1} (shown in Fig. 5)
†3 Observed degradation of n-index in TSC simulation
†4 Destabilization of positional instability due to degradation Δn
†5 Resultant growth rate of enhanced positional instability

of pure positional instability γ is 430 s^{-1}, the degradation of Δn=−0.4 provides an enhancement of growth rate of $\Delta\gamma$=450 s^{-1}. Moreover, because of the strong dependence of positional instabilities on the n-index, even if the degradations of Δn are the same, the growth rate for the plasma with a higher elongation is more enhanced than the plasma with less elongation. For example, the degradations of the elongated configuration of n=−1.6 and the fictitious one of n=−2.1 are approximately the same, Δn=−0.3, however, the resultant destabilizations are $\Delta\gamma$=70 s^{-1} for n=−1.6 and $\Delta\gamma$=150 s^{-1} for n=−2.1, respectively. From these considerations, it follows that the observed degradation Δn is one of the acceleration mechanism of the I_p quench-induced VDE.

Notice that in Table 1 the not yet identified part of VDE rate, that is, $\gamma^*-(\gamma+\Delta\gamma)$, still remains about 200 s^{-1} for all configurations, which is comparable in size to the VDE rate γ^* of a circular configuration. Since the circular plasma should be marginally stable against both vertical displacement and radial expansion modes, we deduce that all VDE-like behavior of 200 s^{-1} is not due to an enhancement of positional instability but instead caused by an imbalance of attractive forces arising from the asymmetric JT-60U vacuum vessel.

2. VDE due to β_p Collapse

(1) TSC Simulation

In order to cause a β_p collapse in the high β_p plasma with β_p=1.7, I_p=1.5 MA, l_i=1.5 and the plasma shape of κ=1.5, δ=0.14 and n=−1.5, we introduced a rapid plasma pressure drop, which triggers the β_p collapse-induced VDE. The electron temperature T_e after the β_p collapses was still sufficiently high (>3 keV) to prevent the I_p quench-induced VDE. Three β_p collapses lasting for 200 μs were chosen: $\Delta\beta_p$=−0.5, −1.0 and −1.5. That is, the β_p values just after β_p collapses were decreased to 1.2, 0.7, and 0.2, respectively. **Figure 6** shows TSC time-traces of the magnetic axis on a poloidal plane during the period of 5.0 ms from the onset of the β_p col-

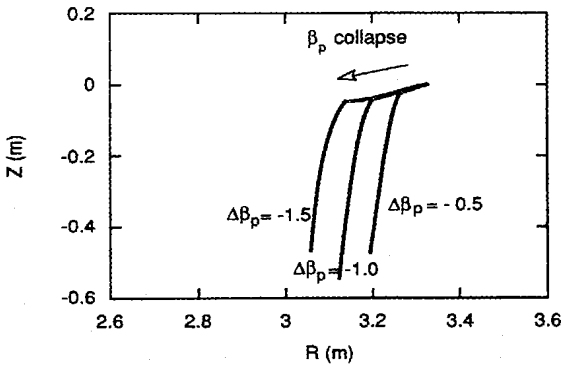

$\Delta\beta_p$: Severity of β_p collapse of initial plasma (n=−1.5) with I_p=1.5 MA, β_p=1.7 and l_i=1.5

Fig. 6 TSC time-traces of plasma magnetic axis on poloidal plane during 5 ms evolution of β_p collapse-induced VDE in JT-60U tokamak

lapse. The plasma location before the β_p collapse was positioned at (3.33 m, 0.0 m). All the plasmas moved downward to around Z=−50 cm at 5 ms after the β_p collapse, that is, the VDE dynamics after β_p collapses are similar each other. The plasma current remained constant in time, although the radial shift due to the β_p collapse led to a small increment of ΔI_p<0.1 MA at 200 μs. Although the triangularity δ decreased largely coinciding with the β_p collapse, the vertical displacement after the β_p collapse did not accompany both the plasma deformation and the relaxation of current profile until 4 ms, that is, the displacement during the VDE is nearly rigid.

During the initial period of 200 μs, the β_p collapse leads to coincident radial shifts ΔR of the magnetic axis, which were nearly proportional to $\Delta\beta_p$: *i.e.*, ΔR=−5.5 cm for $\Delta\beta_p$=−0.5, ΔR=−12.0 cm for $\Delta\beta_p$=−1.0, and ΔR=−18.0 cm for $\Delta\beta_p$=−1.5. In every case, the β_p collapse provides a small amount of coincident downward displacement. The mechanism of the downward perturbation initiating the VDE in bottom-diverted SN tokamaks has been discussed in detail elsewhere[5].

The β_p collapse is observed to produce an instantaneous n-index degradation Δn of the vertical field at the magnetic axis. **Figure 7** shows TSC time-histories of the n-index and the VDE evolution. A radial shift of the plasma induces a restoring eddy current on the resistive shell. The eddy current on the inboard resistive shell flows in the opposite direction to the plasma current, whereas the eddy current on the outboard shell flows in the same direction. Consequently, the vertical magnetic field at the plasma decreases and the radial shift can be suppressed. Such distribution of eddy currents provides an additional quadrupole moment of the magnetic field in the plasma region, causing the n-index to degrade. The n-index degradation remained nearly constant in time for the period of TSC simulations, because the induced eddy current persists during the L/R time

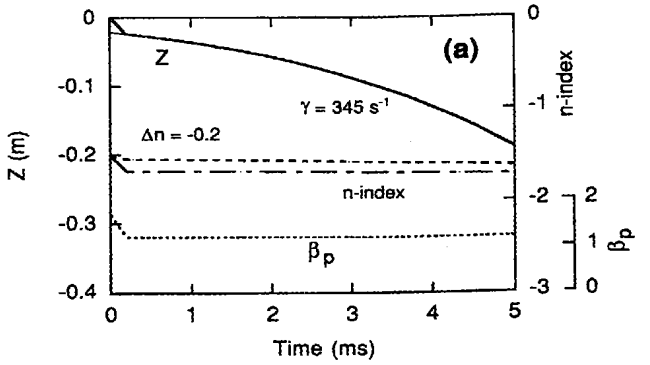

(a) β_p collapse-induced VDE due to collapse of $\Delta\beta_p$=−0.5

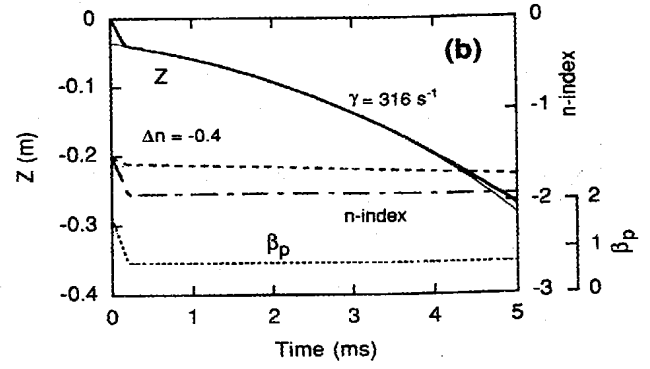

(b) β_p collapse-induced VDE due to collapse of $\Delta\beta_p$=−1.0

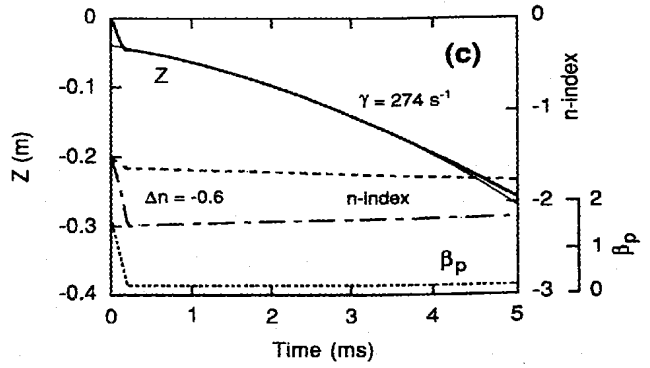

(c) β_p collapse-induced VDE due to collapse of $\Delta\beta_p$=−1.5

Dotted line: Δn without contribution of eddy current
Broken line: Δn with contribution of eddy current

Fig. 7 TSC time-evolutions of measured n-index Δn at plasma magnetic axis and VDE dynamics in JT-60U tokamak

of the resistive shell (~8 ms). The magnitudes of Δn are −0.2 for $\Delta\beta_p$=−0.5, −0.4 for $\Delta\beta_p$=−1.0, and −0.6 for $\Delta\beta_p$=−1.5, respectively. The observed VDE rates were estimated to be 345 s^{-1} for $\Delta\beta_p$=−0.5, 316 s^{-1} for $\Delta\beta_p$=−1.0, and 274 s^{-1} for $\Delta\beta_p$=−1.5, all of which are slower than the usual positional instability (375 s^{-1}). Therefore, in the JT-60U tokamak, the β_p collapse does not accelerate the vertical instability, although the significant degradations of the n-index were observed. The TSC result and the simple stability theory[11] apparently

contradict each other. Next, we give a more detailed discussion of the β_p collapse-induced VDE.

(2) VDE Mechanism

Figure 8 shows the linear growth rate of positional instabilities as a function of the decay n-index. Major plasma parameters are I_p=1.5 MA and l_i=1.5. We considered plasmas with β_p=1.7, 1.2, 0.7 and 0.2. The location R of the magnetic axis for β_p=1.7 was 3.33 m, which corresponds to the radial location prior to the β_p collapse. The R for β_p=1.2 was 3.28 m, the R for β_p=0.7 was 3.21 m, and the R for β_p=0.2 was 3.15 m, corresponding to the radial locations just after the collapses of $\Delta\beta_p$=−0.5, −1.0 and −1.5, respectively. All the vertical locations Z were positioned on the midplane (Z=0.0 m).

Figure 8 indicated clearly both that the n-index degradation leads to higher growth rates of positional instabilities and that the high β_p plasma is more unstable than the low β_p plasma. In Fig. 7(c), we have observed the n-index degradation of Δn=−0.6 caused by the collapse of $\Delta\beta_p$=−1.5. The resultant n-index was −2.1, and the VDE rate was 274 s^{-1}. Here, we attempt to understand the acceleration mechanism of the β_p collapse-induced VDE using Fig. 8. First, follow the path (1) along the vertical line of n=−1.5, and next, follow the path (2) along the curve of the growth rate for β_p=0.2. The path (1) corresponds to the collapse of $\Delta\beta_p$=−1.5, and results in an improvement of the positional instability due to the loss of the plasma pressure. The second path (2) corresponds to the enhancement of positional instability due to the degradation of Δn=−0.6. In following the path (1), the effect of coincident n-index degradation is neglected. The n-index degradation is taken into account only in the second path (2). Therefore, the growth rate of positional instability of the plasma with β_p=0.2, and n=−2.1 is obtained to be $\gamma\sim$290 s^{-1} at the radial location of R=3.15 m, that is nearly same as the β_p collapse-induced VDE of 274 s^{-1}. For the cases of $\Delta\beta_p$=−0.5, and −1.0, a similar procedure provides also almost the same enhancements of positional instabilities as are shown in Figs. 7(a) and (b), respectively.

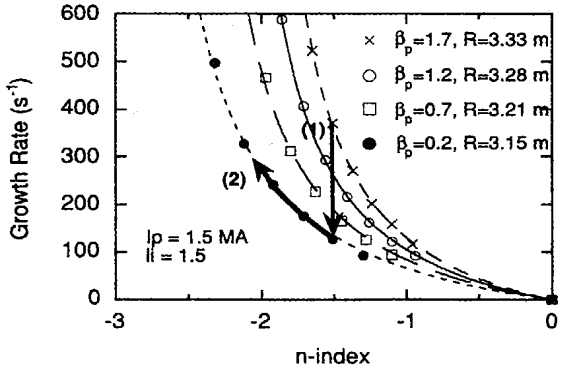

(1): Path corresponding to collapse of $\Delta\beta_p$=−1.5
(2): Path corresponding to destabilization of positional instability due to degradation of Δn=−0.6

Fig. 8 Linear growth rates of JT-60U positional instabilities as a function of n-index

As a consequence of these considerations, we can conclude the mechanism of the β_p collapse-induced VDE in the JT-60U tokamak as follows: Although the n-index degradation owing to the eddy current induced in the resistive shell can accelerate the positional instabilities, the loss of plasma pressure improves the positional instability. In the JT-60U tokamak, the improvement offsets the destabilization. The n-index degradation caused by the β_p collapse depends strongly on the shell-geometry. Therefore, the acceleration mechanism of β_p collapse-induced VDEs depends strongly on the specifics of the shell-geometry, and a variety of VDE characteristics will be seen in high β_p tokamaks with a variety of resistive shells.

IV. Amelioration and Deterioration of VDEs

1. VDE Amelioration in JT-60U Tokamak

In the preceding section, it was clarified that in a mildly elongated low β_p tokamak the important acceleration mechanism of I_p quench-induced VDEs is the imbalance of attractive forces arising from the up-down asymmetry of the shell-geometry, and that the n-index degradation during the I_p quench has only a minor effect on the VDE acceleration. Therefore, if the imbalance attractive force can be removed, then the I_p quench-induced VDE would not be expected to occur in a mildly elongated tokamak.

(1) Neutral Position

Figure 9 shows the vertical displacement of the magnetic axis at 1.0 ms after energy quench followed by the I_p quench of 50 s^{-1}, as obtained by the TSC simulations. Major plasma parameters of the initial equilibria are as follows: plasma current I_p=700 kA, poloidal beta β_p=0.2, and plasma internal inductance l_i=1.5. The initial vertical location Z of the magnetic axis is positioned between −50 cm and 30 cm. The n-index is

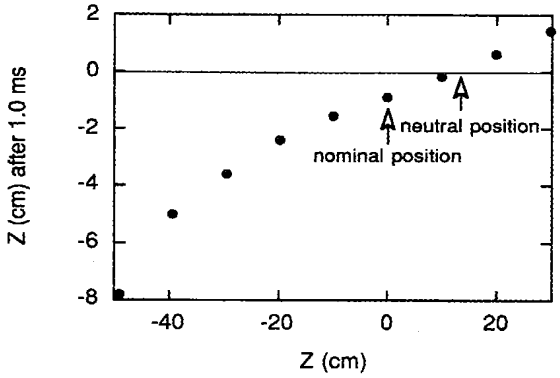

Fig. 9 Vertical displacement of plasma magnetic axis at 1.0 ms after energy quench followed by I_p quench of 50 s^{-1} (I_p=700 kA, β_p=0.2, l_i=1.5)

about −1.0, therefore the up-down imbalance of attractive forces dominates the VDE dynamics. It is seen that the VDE always evolves along a predictable direction, *i.e.*, upward or downward. Especially significant is that there is a neutral equilibrium location about 15 cm above the JT-60U midplane. When the plasma is positioned at the neutral location before an energy quench, the effective VDE rate can be zero. Above this neutral location, the plasma is always attracted upward, while below this location the plasma is always attracted downward. The speed of the vertical shift becomes faster as the distance of the magnetic axis from the neutral location increases. These results reflect the typical characteristics of VDE dynamics caused by the imbalance of attractive forces. As was mentioned, the lower part of the cross section of the JT-60U vacuum vessel is slightly deformed on the inside, therefore the neutral equilibrium location of 15 cm indicated in Fig. 9 is reasonable.

(2) Amelioration Performance of I_p Quench-Induced VDE

In the JT-60U tokamak, it has been experimentally demonstrated that the optimization of the vertical location of the predisruption equilibria is quite effective in suppressing the onset of VDEs[20]. **Figure 10** presents a VDE amelioration demonstration during a disruption without any active feedback control. During the rapid (15 ms) I_p quench, the vertical excursion of the magnetic axis was kept small, within ±2 cm of the initial position of 15 cm above the midplane, consistent with the TSC result. Notice that in a mildly elongated tokamak there should always be a neutral equilibrium location, and that one can soften I_p quench-induced VDEs by optimizing the vertical location of the predisruption equilibria. In an up-down symmetric tokamak, the neutral equilibrium location lies on the midplane.

2. Numerical Evidence of VDE Deterioration

In Chap.III, we pointed out that the dynamics of the β_p collapse-induced VDE is characterized by the competitive mechanisms of the destabilization of positional instability due to the n-index degradation and the self-recovery of positional stability due to the loss of the plasma pressure. It was also shown that the destabilization depends strongly on the geometry of the resistive shell. In the JT-60U tokamak, we have never observed any enhancement of VDEs caused by the β_p collapse, therefore the vacuum vessel is considered to have a favorable stabilizing effect on the β_p collapse-induced VDE. In the following, we discuss the effect of the shell-geometry on the VDE dynamics.

(1) Extremely Fast β_p Collapse-Induced VDE

Figure 11 illustrates the TSC conductors that model the PF coil system (represented by open boxes) and the resistive shell (closed boxes). The PF coil system is identical with that of the JT-60U. Therefore, the plasma configurations are also same as the high β_p plasma used in Chap.III, *i.e.*, the vertically elongated (n=−1.5), bottom-diverted, SN plasma with I_p=1.5 MA, β_p=1.7, l_i=1.5 with a plasma shape of κ=1.5 and δ=0.14. The location of the magnetic axis before the β_p collapse is positioned at (3.33 m, 0.0 m). The resistive shell with a decay time constant of about 18 ms is up-down symmetric with respect to the midplane. The shell-geometry is typical of those commonly used in computational studies on controlling the positional instability[21]. The growth rate of positional instability including the shell effect is calculated to be 149 s^{-1} using TSC.

Figure 12 shows the TSC time-traces of the magnetic axis on a poloidal plane during the period of 5.0 ms from the onset of the β_p collapse. Three β_p collapses were studied with $\Delta\beta_p$=−0.5, −1.0 and −1.5 each occurring on a time scale of 200 μs. The coincident radial shifts ΔR of the magnetic axis at 200 μs were nearly proportional to the severity of the β_p collapse, *i.e.*, ΔR=−7.5 cm for $\Delta\beta_p$=−0.5, ΔR=−13.8

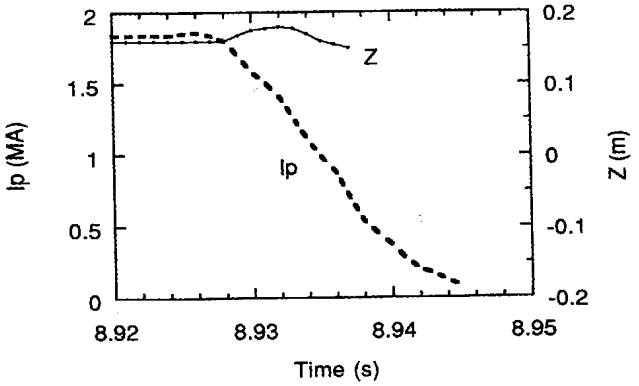

Fig. 10 VDE amelioration performance in JT-60U disruptive discharge after optimizing the plasma vertical location at Z=+15 cm

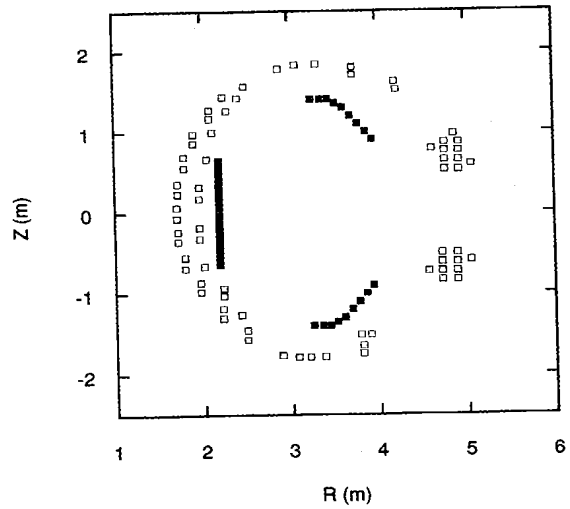

Open box: PF coil system identical with JT-60U tokamak
Closed box: Resistive shell up-down symmetric with respect to midplane

Fig. 11 TSC configuration of model tokamak

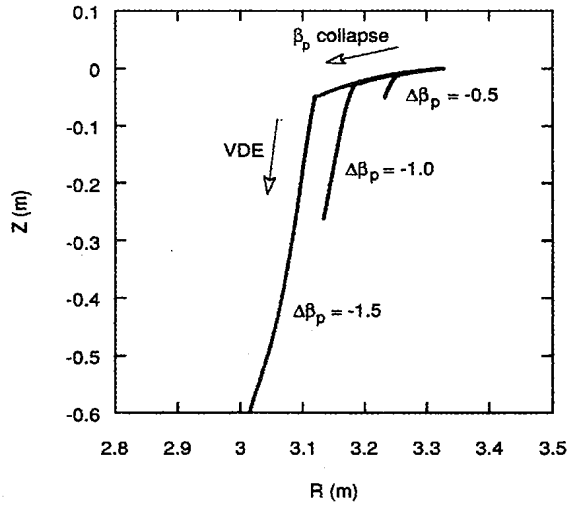

$\Delta\beta_p$: Severity of β_p collapse of initial plasma (n=−1.5) with I_p=1.5 MA, β_p=1.7 and l_i=1.5

Fig. 12 TSC time-traces of plasma magnetic axis on poloidal plane during 5 ms evolution of β_p collapse-induced VDE in model tokamak

cm for $\Delta\beta_p$=−1.0, and ΔR=−21.5 cm for $\Delta\beta_p$=−1.5. Extremely fast VDEs were observed in the cases of $\Delta\beta_p$=−1.5 and −1.0. For $\Delta\beta_p$=−1.5, a large vertical displacement of Z=−1.06 m was obtained 5.0 ms after the β_p collapse. For $\Delta\beta_p$=−1.0, the plasma moved downward to Z=−26.2 cm at 5 ms. For $\Delta\beta_p$=−0.5, the vertical position remained close to the initial location (Z=−5.0 cm at 5.0 ms). Figure 12 shows clearly that a strong β_p collapse can induce an extremely fast VDE without an I_p quench, and that the VDE becomes much faster as the severity of the β_p collapse increases.

The β_p collapse is observed to produce an instantaneous degradation Δn of the n-index at the magnetic axis. **Figure 13** shows TSC time-histories of the n-index and the VDE evolution. At 200 μs, the magnitudes of Δn are −0.3 for $\Delta\beta_p$=−0.5, −0.6 for $\Delta\beta_p$=−1.0, and −1.1, for $\Delta\beta_p$=−1.5, respectively. The observed VDE rates were estimated to be 237 s^{-1} for $\Delta\beta_p$=−0.5, 426 s^{-1} for $\Delta\beta_p$=−1.0, and 655 s^{-1} for $\Delta\beta_p$=−1.5, which is almost five times faster than the positional instability (149 s^{-1}). In what follows, we discuss in detail the acceleration mechanism of the β_p collapse-induced VDE observed in the model tokamak of Fig. 11.

(2) Effect of Shell-Geometry

Figure 14 shows the linear growth rate of positional instabilities of the model tokamak as a function of the n-index. Major plasma parameters are I_p=1.5 MA, l_i=1.5 and a variety of β_p=1.7, 1.2, 0.7 and 0.2. The radial location R of the magnetic axis for β_p=1.7 is 3.33 m, which corresponds to the location prior to the β_p collapse. The R for β_p=1.2 is 3.26 m, the R for β_p=0.7 is 3.19 m, and the R for β_p=0.2 is 3.11 m, corresponding to the radial locations just after the collapses of $\Delta\beta_p$=−0.5, −1.0 and −1.5, respectively. All the vertical locations Z are positioned on the midplane (Z=0.0 m). Using Fig. 14, we can obtain a growth rate consistent with the VDE enhancement for $\Delta\beta_p$=−1.5 seen in Fig. 13(c), where the resultant n-index due to the degradation Δn of −1.1 was −2.6, and the enhanced VDE rate was 655 s^{-1}. By following the sequence of the path (1) and the path (2) in Fig. 14 as well as the procedure used in Chap.III, we obtain the growth rate of the β_p collapse-induced VDE as $\gamma\sim$670 s^{-1} at the radial location R=3.11 m. In the cases of $\Delta\beta_p$=−0.5 and −1.0, a similar procedure provides

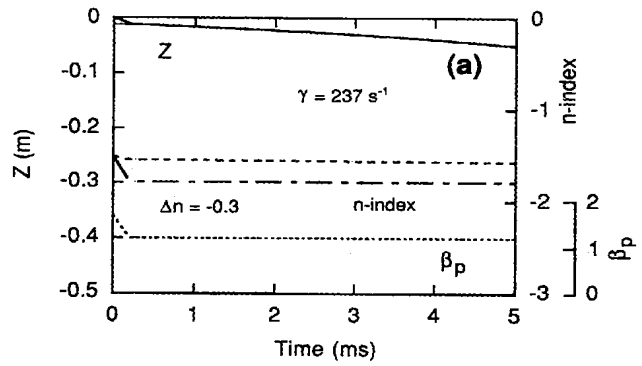

(a) β_p collapse-induced VDE due to collapse of $\Delta\beta_p$=−0.5

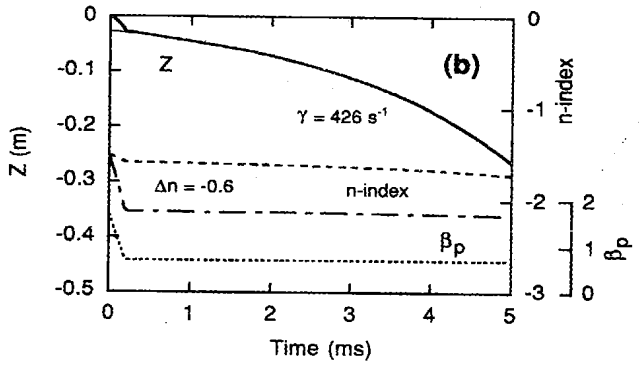

(b) β_p collapse-induced VDE due to collapse of $\Delta\beta_p$=−1.0

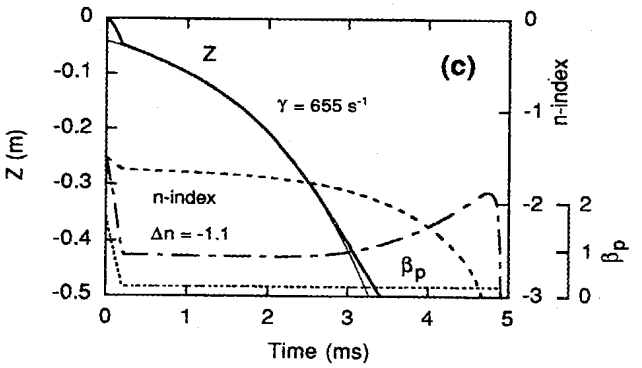

(c) β_p collapse-induced VDE due to collapse of $\Delta\beta_p$=−1.5
Dotted line: Δn without contribution of eddy current
Broken line: Δn with contribution of eddy current

Fig. 13 TSC time-evolutions of measured n-index Δn at plasma magnetic axis and VDE dynamics in model tokamak

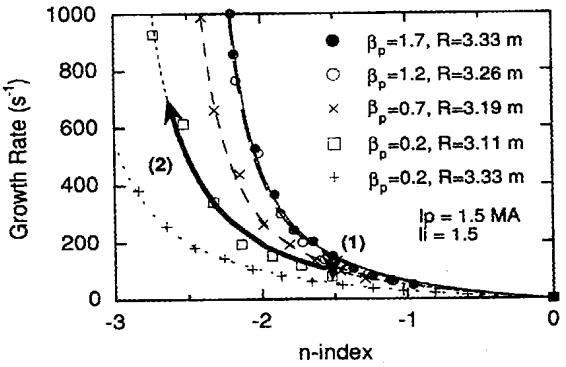

(1): Path corresponding to collapse of $\Delta\beta_p$=−1.5
(2): Path corresponding to destabilization of positional instability due to degradation Δn=−1.1

Fig. 14 Linear growth rates of positional instabilities *vs.* n-index in model tokamak

almost the same enhancement of the positional instability as is shown in Figs. 13(a) and (b), respectively.

In Fig. 14, we have presented supplementary TSC results on the linear growth rate of the positional instability of a plasma with β_p=0.2 and l_i=1.5. The radial location R is 3.33 m, which corresponds to the location prior to the β_p collapse. The difference of the growth rates between plasmas with the same plasma parameters but with the different radial positions of R=3.33 m and R=3.11 m can be seen. Notice that the plasma positioned on an inward side is more unstable than the plasma positioned on an outward side. Utilizing Eq.(6), the stability index n_s of the plasma at R=3.11 m is estimated to be 14% less than the one at R=3.33 m. We can obtain a similar reduction of the stability index n_s evaluated from Fig. 14 by means of the least squares fitting with the form of Eq.(4), that is, the stability index n_s of the plasma at R=3.11 m was estimated to be 12% less than the one at R=3.33 m. Therefore, it follows that the inward radial shift due to the loss of plasma pressure leads to the reduction of the stability index n_s and results in a significant destabilization of the positional instability.

The underlying mechanisms, which characterize the β_p collapse-induced VDE, are summarized as follows: (a) The loss of plasma pressure improves the positional instability. (b) The inward radial shift of the magnetic axis due to a β_p collapse results in a destabilization owing to the reduction of the stability index n_s. (c) The eddy current on a resistive shell induced by the strong β_p collapse degrades the n-index and leads to a significant destabilization. The mechanisms (b) and (c) depend on the specifics of the shell-geometry, and compete with the improvement (a) during disruptions. Consequently, it follows that the optimization of the shell-geometry is quite important in order to avoid a β_p collapse-induced VDE. For the shell-geometry of the JT-60U, which completely encloses the plasma, the inward radial shift due to a β_p collapse was kept to be −18 cm (−22 cm in the model tokamak) and the n-index degradation was ameliorated to be −0.6 (−1.1 in the model tokamak). Consequently, the JT-60U vacuum vessel plays a superior role of stabilizing the β_p collapse-induced VDE.

V. Conclusions

Mechanisms that govern VDEs during disruptions have been investigated using the TSC code in order to add to our understanding of tokamak disruption dynamics. The goal is to learn to operate disruption-free discharges, or at least to avoid hard disruptions by soft landing.

Typical disruption events such as the β_p collapse and the subsequent I_p quench accelerate VDEs due to the destabilizing effect of the resistive shell, which has previously been thought to stabilize VDEs. The adverse effect is due to two different effects. The first is the significant destabilization of the positional instability arising from a large and sudden degradation of the decay n-index in addition to a reduction of the stability index n_s. The second is the intense acceleration arising from an up-down imbalance of attractive forces owing to the asymmetry of the shell-geometry. In highly elongated plasmas, the destabilization of the positional instability is a dominant acceleration mechanism both of the β_p collapse-induced VDE and the I_p quench-induced VDE. In a tokamak with a mild elongation, an I_p quench-induced VDE is mainly dominated by the imbalance of the attractive force.

The shell-geometry significantly affects the VDE dynamics. In JT-60U, it has been demonstrated that positioning the plasma at a neutral location can successfully avoid the I_p quench-induced VDE. Moreover, the JT-60U vacuum vessel was shown to be well suited to prevent the β_p collapse-induced VDE. Therefore, even for the worst case in which a rapid I_p quench occurs immediately after a strong β_p collapse, the I_p quench-induced VDE enhanced by the β_p collapse will not be dangerous in the JT-60U plasma at a neutral position. For example, if a collapse of $\Delta\beta_p$=−1.5 provides the n-index degradation of Δn=−0.6, and an immediate I_p quench of 40 s^{-1} provides the additional degradation of Δn=−0.3, then the resultant VDE rate is estimated as γ=550 s^{-1} at the total n-index of n=−2.4. This is only 1.5 times larger than the pure positional instability (375 s^{-1}). However, in the model tokamak, such a major disruption leads to a despairing VDE, whose growth rate can be predicted about 20 times larger than the pure positional instability.

The newly identified VDE mechanisms have significant implications for designing a next-generation tokamak reactor like ITER, in which the active feedback system is incapable of preventing the VDE, and a large Halo current will be induced. We propose the following design strategy: First, careful optimization of the

allowable plasma elongation is a crucial issue, *i.e.*, considering the impact of disruptions, a mildly elongated tokamak is always more benign than a highly elongated tokamak. Therefore, the allowable plasma elongation guide-lines must be conservative, even at the expense of better confinements and improved beta limits. Second, in order to minimize the force imbalance due to the I_p quench, optimization of the vertical position of plasma equilibrium is required. Maintaining up-down symmetry of the resistive shell with respect to the midplane is preferred, otherwise further effort is necessary to seek the neutral location. Third, in order to mitigate a β_p collapse-induced VDE, the shell-geometry must be optimized to keep the inward radial shift of the magnetic axis small and to ameliorate the n-index degradation. Having the resistive shell completely enclosing the plasma like the JT-60U vacuum vessel is desirable.

Acknowledgments

The authors wish to thank the members of the Japan Atomic Energy Research Institute who have contributed the JT-60U project, and are indebted to colleagues from the JT-60U group for making their data freely available. They are most grateful to Drs. T. Hirayama and H. Kishimoto for their continuous encouragements. Useful discussions with Drs. M. Azumi and T. Tsunematsu are also acknowledged. The authors would like to express their gratitudes to Drs. M. Sugihara and G. Kurita for their fruitful comments on the physical meaning of the stability index n_s.

References

(1) Yoshino, R., *et al.*: *Nucl. Fusion*, **33**, 1599 (1993).
(2) Sayer, R.O., *et al.*: *ibid.*, **33**, 969 (1993).
(3) Yoshino, R., *et al.*: *Proc. 15th Int. Conf. Plasma Physics and Controlled Nuclear Fusion Research, Seville, Spain, Sep. 26 - Oct. 1, 1994*, IAEA, Vienna, Vol.1, p.685 (1995).
(4) Taylor, P.L., *et al.*: *Phys. Rev. Lett.*, **76**, 916 (1996).
(5) Kellman, A.G., *et al.*: *Proc. 16th Symp. on Fusion Technol., London, Sep. 3-7, 1990*, Elsevier Sci. Publ., Vol.2, p.1045 (1991).
(6) Gruber, O., *et al.*: *Plasma Phys. Contr. Fusion*, **34**, B191 (1993).
(7) Merrill, B.J., Jardin, S.C.: *Fusion Eng. Des.*, **5**, 235 (1987).
(8) Thomas, P.R., *et al.*: *Proc. 10th Int. Conf. Plasma Physics and Controlled Nuclear Fusion Research, London, Sep. 12-19, 1984*, IAEA, Vienna, Vol.1, p.353 (1985).
(9) Ward, D.J., Jardin, S.C.: *Nucl, Fusion*, **32**, 973 (1992).
(10) Nakamura, Y.: *Jpn. J. Appl. Phys.*, **25**, 1575 (1986).
(11) Fukuyama, A., *et al.*: *ibid.*, **14**, 871 (1975).
(12) Rebut, P-H., *et al.*: Presented at 15th Int. Conf. Plasma Physics and Controlled Nuclear Fusion Research, Seville, Spain, Sep. 26 - Oct. 1. 1994, IAEA-CN-60/E-1-I-1.
(13) Neyatani, Y., *et al.*: *Fusion Technol.*, **28**, 1634 (1995).
(14) Pick. M.A., *et al.*: *Proc. 14th Symp. Fusion Engineering, San Diego, CA, Sep. 30 - Oct. 3, 1991*, IEEE, New York, Vol.1, p.187 (1992).
(15) Jardin, S.C., *et al.*: *J. Comput. Phys.*, **66**, 481 (1986).
(16) Pautasso, G., *et al.*: *Nucl. Fusion*, **32**, 455 (1994).
(17) Miyamoto, K.: "*Plasma Physics for Nuclear Fusion*", MIT Press, (1980).
(18) Nakamura, Y., *et al.*: *Nucl. Fusion*, **36**, 643 (1996).
(19) Nakamura, Y., *et al.*: β_p collapse-induced vertical displacement event in high β_p tokamak disruption, To be published in *Plasma Phys. Contr. Fusion.*
(20) Yoshino, R., Nakamura, Y., Neyatani, Y.: *Nucl. Fusion*, **36**, 295 (1996).
(21) Ward, D.J.: Studies of feedback stabilization of axisymmetric modes in deformable tokamak plasmas, PhD Thesis, Princeton Univ., Princeton, NJ, (1990).